Date 2012
Author Loo, S. van, T.J.C. van Terwisga, H.W.M. Hoeijmakers, And M. Hoekstra
Address Delft University of Technology
Ship Hydromechanics and Structures Laboratory
Mekelweg 2, 2628 CD Delft

TUDelft

Delft University of Technology

Numerical study on collapse of a cavitating cloud of bubbles

by

Loo, S. van, T.J.C. van Terwisga, H.W.M. Hoeijmakers and M. Hoekstra

Report No. 1888-P **2012**

Proceedings of the International Symposium on Cavitation, CAV2012, 13-16 August 2012, Singapore, ISBN: 978-981-07-2826-7.

Proceedings of the

8th International Symposium on Cavitation

13 – 16 August 2012
Singapore

ISBN: 978-981-07-2826-7

Editors

Claus-Dieter Ohl, Evert Klaseboer, Siew Wan Ohl, Shi Wei Gong and B. C. Khoo

Published by

RESEARCH PUBLISHING

Hosted by

Sponsors

Bubbly Flows and Cloud Cavitation

BACK

Numerical

- **Development of a Nonlinear Asymptotic Method for Calculation of Nearly Axisymmetric Cavitation Flows**
  V. N. Buyvol and V. V. Serebryakov

- **Efficient Numerical Simulation of Unsteady Cavitating Flows Using Thermodynamic Tables**
  F. Khatami, A. H. Koop, E. T. A. van der Weide and H. W. M. Hoeijmakers

- **Evaluation of Cavitation Models for Prediction of Transient Cavitating Flows around a Stationary and a Pitching Hydrofoil**
  Biao Huang, Antoine Ducoin and Yin Lu Young

- **Features of Nucleation and Growth of Gas Bubbles in Magmas**
  Davydov Maxim

- **Further Improvement of Bubble Model for Cavitating Flow Simulations**
  Yoshiaki Tamura, Nobuo Tsurumi and Yoichiro Matsumoto

- **Growth and Collapse of Laser Generated Bubbles Near a Curved Density Interface**
  Mark Esson

- **MGFM Applied to Underwater Explosion near a Thin Plate with Cavitation Evolution**
  Liu Tiegang, Feng Chengliang and Xu Liang

- **Modeling Cavitation Flow of Cryogenic Fluids with Thermodynamical Phase-Change Theories**
  Zhang XiaBin, Wei Zhang and Qiu LiMin

- **Modelling the Total Monomeric Anthocyanin (TMA) Extracted From Mangosteen Hull in Ultrasonic Assisted Acidified Aqueous Solvent Extractions**
  C. Y. Cheok N. L Chin, Y. A. Yusof, R. A. Talib and C. L Law

- **MTBE-Degradation by Hydrodynamic Induced Cavitation**
  Andreas Schmid

- **Non-Singular Boundary Integral Method and Its Applications to Oscillating Bubbles**
  Qiang Sun, Evert Klaseboer, Boo Cheong Khoo and Derek Y. C. Chan

- **Numerical Analysis for Influence of Cascade Solidity on the Performances of Cavitating Inducers**
  Li Xiaojun, Yuan Shouqi, Pan Xiwei and Pan Zhongyong

- Numerical Analysis for Influence of Cascade Solidity on the Performances of Cavitating Inducers
  Li Xiaojun, Yuan Shouqi, Pan Xiwei and Pan Zhongyong

- Numerical Analysis of Axisymmetric Supercavitating Flows
  Byoung-Kwon Ahn, Hyun-Gil Jang, Hyoung-Tae Kim and Chang-Sup Lee

- Numerical Investigations of Nonspherical Bubble Collapse Near Boundaries by the Improved Ghost Fluid Method
  Yoshinori Jinbo, Toshiyuki Ogasawara and Hiroyuki Takahira

- Numerical Method for the Analysis of Cavitating Waterjet Propulsion Systems
  Shu-Hao Chang and Spyros A. Kinnas

- Numerical Simulation and Analysis of Cavitating Flow in a Centrifugal Pump
  Dongxi Liu, Houlin Liu, Yong Wang, Suguo Zhuang, Jian Wang and Du Hui

- Numerical Simulation of Cavitation around a Two-Dimensional Hydrofoil using VOF Method and LES Turbulence Model
  Ehsan Roohi, Amir Pouyan Zahiri and Mahmud Pasandideh-Fard

- Numerical Simulation of Cavitation Flow Around a Hydrofoil
  Houlin Liu Jian Wang, Bixing Yin, Yong Wang, Suguo Zhuang and Dongxi Liu

- On the Capability of a RANS Method to Assess the Cavitation Erosion Risk on a Hydrofoil
  Ziru Li and Tom Van Terwisga

- Performance Assessments for Various Numerical Cavitation Models using Experimental Data
  Yaw-Huei Lee, Jing-Chin Tu, Yu-Chi Chang and Yi-Chih Chow

- Periodic Phenomena on a Partially Cavitating Hydrofoil
  Anne Gosset, Marcos Lema and Fernando López Peña

- Phase Change Model based on the Idea of Apparent Phase Equilibrium in Unsteady Cavitating Flow
  Yuka Iga

- Prediction of Cavitation on Two- and Three-Dimensional Hydrofoils by an Iterative BEM
  Yasemin Arikan, Fahri Çelik, Ali Doğrul and Şakir Bal

Measurements

Numerical Study on Collapse of a Cavitating Cloud of Bubbles

S. van Loo
University of Twente

T.J.C. van Terwisga
Marin/TU Delft

H.W.M. Hoeijmakers
University of Twente

M. Hoekstra
Marin

SUMMARY

One of the major causes of wear on ship hydrofoils is cavitation. Clouds of interacting bubbles behave nonlinearly and can experience very sudden changes in void fraction. These nonlinear collapsing mechanisms can result in a coherent collapse of bubble clouds which have great damage potential.
In this study the model, proposed by Wang and Brennen [1999], has been implemented. This model employs the fully nonlinear continuum mixture equations coupled with the Rayleigh-Plesset equation. The set of equations is solved using a Lagrangian integral method. The sensitivity of the results for parameters such as the initial void fraction of the cloud, initial cloud size as well as characteristics of the imposed pressure perturbation, has been investigated. Based on results of a RANS method for the flow around a hydrofoil with shedding sheet cavities, an equivalent cavitated cloud and corresponding pressure perturbation has been determined that serves as input for the bubble cloud method.

INTRODUCTION

Cavitation is in a physical sense not fundamentally different from boiling. In a boiling process, vapor forms in a fluid because the temperature of the fluid is raised to the saturated vapor/liquid temperature. This results in a phase change from liquid to vapor

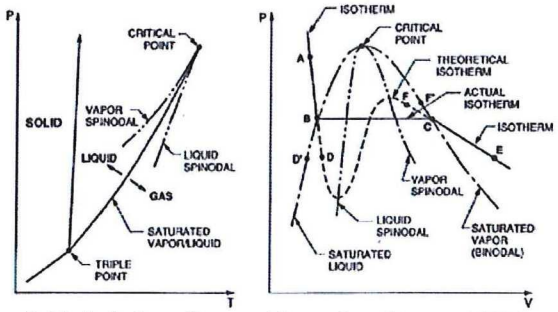

Figure 1: Typical phase diagram. Figure from Brennen [1995]

In figure 1 a typical phase diagram is shown on the left. When a liquid is heated the saturated vapor/liquid line is passed at a certain point where the liquid will become vapor.When one considers a liquid, it can be seen that when the pressure is lowered, the same saturated vapor/liquid line is passed. This process in which a phase change results from the lowering of pressure is called cavitation. On the right of figure 1 a line of constant temperature (isotherm) is plotted in the pressure specific volume plot. Since the density of vapor is much lower than that of liquid an expansion will take place when the pressure is dropped below the saturated vapor pressure, point B in the graph, and vapor is formed. Only if enough nucleation sites are available the isotherm will go straight from point B to C, where all the liquid is now vapor and the pressure can drop further in the vapor phase. If no or a small number of nucleation sites are available, pressure could be lowered below the saturated vapor pressure, according to the theoretical isotherm BD. The location of first rupture is the weakest spot in the fluid. The process in which a microscopic void starts to grow to a macroscopic bubble is called inception. Inception happens at weak places in a liquid, called nucleation sites. If these nucleation sites are microscopic voids that are available in the fluid due to thermal effects, we speak of homogeneous nucleation. However, it is more likely that weak spots appear at solid boundaries within the flow regime. In this case we speak of heterogeneous nucleation. Another possible nucleation site is a microscopic bubble that contains contaminant gas.

A pressure decrease may occur for two reasons. The overall pressure is decreased or the fluid accelerates. In an incompressible inviscid, steady flow, an increase in flow velocity decreases the pressure in the flow field. Examples are the flow over ship propellers and through pump impellers. To describe the relationship between overall pressure, the flow velocity and the likelihood of cavitation, the cavitation number is defined as:

Proceedings of the Eighth International Symposium on Cavitation (CAV 2012)
Edited by Claus-Dieter OHL, Evert KLASEBOER, Siew Wan OHL, Shi Wei GONG and Boo Cheong KHOO.

ISBN: 978-981-07-2826-7 :: doi:10.3850/978-981-07-2826-7_187

$$\sigma = \frac{p_0 - p_v(T_0)}{\frac{1}{2}\rho_L U_0^2} \quad (1)$$

Here p_0 and T_0 are the reference pressure and temperature, respectively, for example in the far-field, and U_0 is the corresponding reference velocity. The quantity $p_v(T)$ is the partial pressure of the vapor and ρ_L is the liquid density. From the cavitation number it can be seen that if the cavitation number is sufficiently large, inception will not occur. This happens if the reference pressure p_0 is sufficiently large or the reference velocity U_0 is sufficiently low. Also, if the reference pressure is low or the reference velocity is high the cavitation number will be low, which results in a flow that is more likely to cavitate. The particular value of σ for which nucleation first starts to occur is called the nucleation cavitation number. The dynamics of individual cavitation bubbles is described by the Rayleigh-Plesset equation. This equation, for a bubble moving with the velocity field, in its simplest form first derived by Rayleigh in 1917, relates bubble pressure p to bubble radius R, bubble wall velocity DR/Dt and bubble wall acceleration D^2R/Dt^2. It reads for a spherical bubbly iso-thermal flow:

$$\frac{1}{2}\sigma\left(\frac{R_0^{3k}}{R^{3k}} - 1\right) - \frac{1}{2}C_p + \frac{2S}{\rho_L U_0^2 R_0}\left(\frac{R_0^{3k}}{R^{3k}} - \frac{R_0}{R}\right) = \left[\frac{3}{2}\left(\frac{DR}{Dt}\right)^2 + R\frac{D^2R}{Dt^2} + 4\nu_L\frac{1}{R}\frac{DR}{Dt}\right]\frac{1}{U_0^2} \quad (2)$$

Here R_0 is a reference bubble size. D/Dt denotes the substantial derivative, k is the polytropic constant of the contaminant (isentropically behaving) gas inside the bubble and $\nu_L = \mu_L / \rho_L$ is the kinematic viscosity of the liquid, with μ_L the dynamic viscosity of the liquid. Furthermore, C_p is the pressure coefficient, defined as:

$$C_p = \frac{p - p_0}{\frac{1}{2}\rho_L U_0^2} \quad (3)$$

Here S is the surface tension, which can be expressed in terms of the Weber number We as:

$$\mathrm{We} = \frac{\rho_L U_0^2 R_0}{S} \quad (4)$$

The derivation of Eq. (2) can be found in many text books.
Not only nucleation and cavitation is a field of active research, but also bubble disappearance or collapse. Once cavitation bubbles are formed in a region of low pressure, the cavitation bubble will be convected with the flow and may enter into a high pressure region. This will result in a bubble that implodes, or collapses. Bubble collapses are a major cause of erosion on hydrodynamic surfaces. A collapsing bubble radiates strong pressure waves which cause highly localized and transient stresses. Repeated collapses cause local fatigue and subsequent erosion of the material. Entire clouds of bubbles can collapse coherently. For instance in case of a ship propeller, a sheet cavity on the leading edge of the hydrofoil sheds clouds of cavitation bubbles. Further downstream but still above the blade of the propeller the cloud may collapse. In a cloud, interacting bubbles can cause the collapse to be more violent than the effect of the individual collapsing bubbles. As a result of the high pressure peaks appearing when bubbles collapse, noise is produced. The radiated acoustic pressure of a bubble can, according to Dowling and Ffowcs Williams [1983], be written as:

$$p_a = \frac{\rho_L}{4\pi r}\frac{d^2V}{dt^2} \quad (5)$$

Here r is the distance from the source to the point of measurement and V is the volume of the collapsing cavity. From this equation it can be seen that noise is created by the volumetric acceleration of the void. This acceleration is largest when the volumetric velocity dV/dt of the void changes from negative to positive sign, and thus when the void volume V is smallest. So this is when the collapse/rebound is the most violent.

Cavitation phenomena are an area of active research, both experimentally and numerically. In experiments details of the cavitation features are captured using new recording techniques like high-speed cameras and Particle Image Velocimetry. On the numerical side, computers are getting more and more powerful enabling more extensive computations. This makes RANS computations of the entire cavitating flow field possible. From the viewpoint of the maritime industry it is most important to find a way to accurately predict cavitation aggressiveness and its potential erosive power. Thus a method is required that predicts periodic or steady cavitation close to the surface of ship propellers, pump impellers, etc. for which damage from cavitation is to be expected. When and where cavitation is to be expected can be computed numerically with the aid of RANS computations. However, a RANS method is not able to accurately predict the final stage of collapse. It is in this stage that the highest pressures are to be expected. It is the aim of the present study is to provide details of the cloud collapse. This is meant to be achieved with the aid of the model proposed by Wang and Brennen [1999] to provide information that RANS computations cannot produce. Then, it could possibly be used as a post-processor for results of RANS numerical simulations. This will provide more detailed information of the aggressiveness of the collapsing cavity.

Therefore the objectives of the present study are: (i) Obtain solutions of the model proposed by Wang and Brennen [1999].
(ii) Perform a sensitivity study in order to be able to recognize situations in which cavity cluster collapses are most aggressive.
(iii) Explore the possibilities for using the implementation as a post-processor for results of RANS numerical simulations, with the purpose of providing details of the cloud cavity collapse.

MODEL CAVITATING CLOUD OF BUBBLES

The model investigated in this paper describes the nonlinear collapsing behavior of a spherical cloud of bubbles. According to Hansson & Mörch [1980] and Mörch [1982]) the collapse involves inward moving shock waves that are enhanced. This indicates the necessity for a model that does not ignore the nonlinear effects in the cloud and should be able to predict the

radiated acoustic energy, and the potential damaging power of a cavitating cloud. The model investigated therefore retains the nonlinear terms in the governing equations.

Consider a spherical cloud of bubbles as depicted in figure 2. It is assumed that the dependent variables depend on r and t only. The liquid surrounding the cloud is assumed incompressible. The radius of the cloud is denoted by $A(t)$, the radial coordinate with r, the individual bubble radius with $R(r; t)$ and the bubble population per unit liquid volume with η. It is assumed that

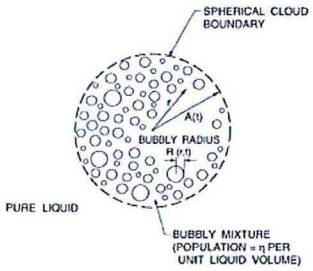

Figure 2: Schematic of a spherical cloud of spherical bubbles. Figure from Wang and Brennen [1999].

coalescence and break-up of the bubbles inside the cloud do not occur and that the bubble distribution is piecewise uniform initially. Also it is assumed that there is no mass transfer through the boundaries of the bubbles. This means that η remains constant and piecewise uniform distributed. Furthermore the bubbles are assumed to be spherical at all times and contain liquid vapor as well as contaminant gas.

At $t = 0$, the cloud is in equilibrium with the surrounding liquid. Then a pressure perturbation $C_{p_\infty}(t)$ is imposed on the pure liquid at infinity and we investigate the reaction of the cloud to this pressure perturbation.

Governing equations

It is assumed that the density of the liquid ρ_L is sufficiently high and the vapor fraction α is sufficiently low to neglect the density of the vapor, i.e. the mixture density becomes:

$$\rho = \alpha\rho_v + (1-\alpha)\rho_L \approx (1-\alpha)\rho_L \qquad (6)$$

In equation (6) α is the fraction of vapor in a unit volume. The volume of an individual bubble is $V_b = \frac{4}{3}\pi R^3$. Then the product ηV_b is the fraction of volume taken up by the bubbles in a unit liquid volume. Noting that the total volume is the liquid volume plus the bubble volume, i.e. equals $V_L(1+\eta V_b)$ we can write for the void fraction:

$$\alpha = \frac{\eta V_b}{1+\eta V_b} \qquad (7)$$

The mixture density then becomes:

$$\rho \approx (1-\alpha)\rho_L = \frac{\rho_L}{1+\eta V_b} \qquad (8)$$

Substitution of Eq. (8) in the continuity equation for the mixture density gives, for the case of spherical symmetry:

$$\frac{1}{r^2}\frac{\partial}{\partial r}(r^2 u) = \frac{12\pi\eta R^2}{3+4\pi\eta R^3}\frac{DR}{Dt} \qquad (9)$$

Here u is the radial velocity and $D/Dt \equiv \partial/\partial t + u\partial/\partial r$.

For the radial component of the momentum equation, neglecting volumetric force fields and viscous stresses, gives:

$$\rho\frac{Du}{Dt} = -\frac{\partial p}{\partial r}$$

Substituting the expression fro the mixture density, Eq. (8) and the expression for the pressure coefficient, Eq. (3), yields:

$$\frac{Du}{Dt} = -\tfrac{1}{6}(3+4\pi\eta R^3)U_0^2\frac{\partial C_p}{\partial r} \qquad (10)$$

The Rayleigh-Plesset equation, Eq. (2), relates the local pressure to the evolution of the radius of the bubble in time. The equation is derived from the momentum equation and a force balance at the edge of a bubble. It is assumed that there is no mass transfer through the bubble boundary, so the content of the bubble does not change. Also, since the bubble is spherical one can make use of spherical symmetry. Note that the equation is derived for a single bubble, making use of a kinematic boundary condition at the edge of the bubble. This will have as a consequence that one should be careful using this equation in calculations in cases for which bubble-bubble interactions are important. Also note that temperature effects are neglected. Finally, it is assumed that the bubble remains spherical at all times.

The variables used in the analysis are non-dimensionalized using the initial bubble size R_0 and the free-stream velocity U_∞, i.e.:

$$\hat{R} = R/R_0;\ \hat{r} = r/R_0;\ \hat{u} = u/U_0;\ \hat{\eta} = \eta R_0^3;\ \hat{t} = tU_0/R_0,$$

Substituting this in the governing equations, and subsequently dropping the hat, yields:

$$\frac{1}{r^2}\frac{\partial}{\partial r}(r^2 u) = \frac{12\pi\eta R^2}{3+4\pi\eta R^3}\frac{DR}{Dt} \qquad (11a)$$

$$\frac{Du}{Dt} = -\tfrac{1}{6}(3+4\pi\eta R^3)\frac{\partial C_p}{\partial r} \qquad (11b)$$

$$\tfrac{1}{2}\sigma(R^{-3k}-1) - \tfrac{1}{2}C_p + \frac{2}{\mathrm{We}}(R^{-3k}-R^{-1}) = \tfrac{3}{2}\left(\frac{DR}{Dt}\right)^2 + R\frac{D^2R}{Dt^2} + \frac{4}{\mathrm{Re}}\frac{1}{R}\frac{DR}{Dt} \qquad (11c)$$

where We is the Weber number, see Eq. (4) and Re is the Reynolds number:

$$\mathrm{Re} = \frac{\rho_L U_0 R_0}{\mu_L} \qquad (12)$$

There are three main causes of damping: effects due to liquid viscosity μ_L; effects due to fluid compressibility through acoustic radiation μ_A; and effects due to thermal conductivi-

ty μ_T, see Chapman and Plesset [1971]. These three components are captured in one effective viscosity which is written as:

$$\mu_E = \mu_L + \mu_T + \mu_A$$

The effective viscosity μ_E will be used in the Rayleigh-Plesset equation to account for the damping mechanisms.

To analyze the equation further, Eq. (11c) is expressed in terms of the bubble-wall acceleration:

$$\frac{D^2R}{Dt^2} = -\frac{3}{2}\frac{1}{R}\left(\frac{DR}{Dt}\right)^2 + \frac{\sigma}{2R}(R^{-3k} - 1) + \frac{2}{\mathrm{RWe}}(R^{-3k} - R^{-1}) - \frac{4}{\mathrm{Re}}\frac{1}{R^2}\frac{DR}{Dt} - \frac{1}{2R}C_p \quad (13)$$

From Eq. (13) it is seen that a negative pressure coefficient ($p < p_\infty$) will result in a positive bubble acceleration, thus growth of the bubble. Note that there are two R^{-3k} terms, both positive to the acceleration. When $R << 1$, which occurs during bubble collapse, these terms will become very large. For instance, when R reaches a value of 0.01, $R^{-3k} \approx 250\times10^6$ for k = 1:4. So in the collapse phase these terms become dominant. Thus, a low value of the bubble radius during collapse results in a very high positive bubble acceleration, and thus a severe rebound.

The Rayleigh-Plesset equation describes the evolution of a single bubble. It does not account for local pressure perturbations experienced by the bubble due to the collapse and rebound of its neighbors. Important parameter in this case is the initial void fraction. The higher the initial void fraction, the closer the bubbles will be to each other, the higher these effects. In the literature (see [Rubinstein, 1985] and [Seo et al., 2010]) it is shown that these effects are of the order of the void fraction. This is a limitation of the model. In the literature there are corrections to the Rayleigh-Plesset equation that make the equation useful up to initial void fraction of O(13%). The local void fraction can, however, be much higher than the initial void fraction. Because the number of bubbles per unit volume liquid is constant, the number of bubbles does not change over time. This means that the error due to bubble interactions is dependent on the initial void fraction, and not the local void fraction. Therefore, one should be careful using initial void fraction much higher than 1%.

Boundary conditions

To solve the three governing equations, Eqs. (11a, b and c), for the three unknown quantities $C_p(r, t)$, $R(r, t)$ and $u(r, t)$ appropriate boundary and initial conditions are required.

For spherically symmetric, incompressible, irrotational flow outside the cloud ($r \geq A(t)$) we can write for the radial velocity can be expressed, dimension-full) as:

$$u(r,t) = \frac{Q(t)}{4\pi r^2}, \text{ with } Q(t) = 4\pi A^2(t)u(A(t),t) \quad (14)$$

or in terms of the velocity potential:

$$\phi(r,t) = -\frac{Q(t)}{4\pi r} \quad (15)$$

Bernoulli's relation for this flow reads:

$$\frac{\partial\phi}{\partial t} + \tfrac{1}{2}u^2 + \frac{p}{\rho_L} = C(t)$$

Upon substitution of Eqs. (14) and (15), and evaluating $C(t)$ at infinity:

$$-\frac{1}{r}\frac{d}{dt}(A^2u) + \tfrac{1}{2}u^2 + \tfrac{1}{2}U_0^2C_p = \tfrac{1}{2}U_0^2C_{p,\infty}(t) \text{ for } r \geq A(t)$$

Then evaluating this expression at the boundary of the cloud it follows, in dimensionless form:

$$C_{p,A}(t) = C_{p,\infty}(t) + \frac{2}{A(t)}\frac{d}{dt}(A^2(t)u_A) - u_A^2 \quad (16)$$

where $u_A = u(A(t),t)$ and $C_{p,A}(t) = \dfrac{p(A(t),t) - p_0}{\frac{1}{2}\rho_L U_0^2}$.

Eq. (16) gives the pressure at the boundary of the cloud that is compatible with the imposed pressure $C_{p,\infty}(t)$ at infinity.

At the center of the cloud there can be no radial motion because of the spherical symmetry of the problem. So the boundary condition is:

$$u(0,t) = 0 \quad (17)$$

Eqs. (16) and (17) are the boundary conditions required for Eqs. (11a) and (11b) for the pressure and velocity inside the clouds. Eq. (11c) for the radius of the bubbles inside the cloud requires just initial conditions.

Initial conditions

For the continuity equation, Eq. (11a) and the momentum equation, Eq. (11b) the initial conditions are, for 0< r <A(0):

$$u(r,0) = 0 \quad (18a)$$

$$C_p(r,0) = 0 \quad (18b)$$

For the bubble radius the initial conditions are:

$$R(r,0) = 1 \quad (19a)$$

$$\frac{DR}{Dt}(r,0) = 0 \quad (19b)$$

$$\frac{D^2R}{Dt^2}(r,0) = 0 \quad (19c)$$

Imposed pressure field at infinity

In Eq (16) the pressure perturbation $C_{p,\infty}(t)$ determines the way in which the cloud will evolve. It is the parameter that can be used to simulate the situation in an experimental setting, or the result of a specific RANS numerical simulation. The pressure perturbation is defined as follows:

$$C_{p,\infty}(t) = \tfrac{1}{2}C_{p,\min}[1 - \cos(2\pi t/t_G)] \quad (20)$$

for 0< t <t_G, and zero otherwise, see figure 3.

For this specific shape two parameters are important: the minimum pressure $C_{P,min}$ and the period of the pressure perturbation t_G. It is noted that when the minimum pressure decreases or the period increases, the response of the cloud will be more severe. To couple this to a cloud passing over an object, the following is noted.

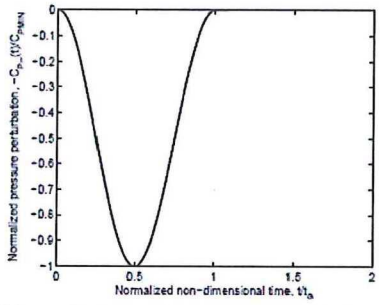

Figure 3: Imposed pressure perturbation $C_{p,\infty}(t)$

The time it would take the cloud to travel with velocity U_0 past a body of length D would be $t = D/U_0$. Substituting this in the expression for dimensionless time yields the order of magnitude of $t_G = D/R_0$. Thus when comparing results of this model to experiments, one can calculate the dimensionless period of the pressure perturbation. The minimum pressure coefficient depends on the case considered.

Numerical approach

In the method of Wang & Brennen [1999] the governing equations are solved in a Lagrangian formulation. In this formulation the local coordinate r moves in time and its value is a function of its initial position r_0, so $r = r(r_0,t)$. The details of the derivation of the equation for the spatial coordinate is given in Wang & Brennen, as well as in van Loo (2011). The resulting expression is:

$$r^3(r_0,t) = \frac{3}{3+4\pi\eta}\int_0^{r_0}[3+4\pi\eta R^3(\xi,t)]\xi^2 d\xi \qquad (21)$$

Differentiation of this Lagrangian coordinate with respect to time gives the radial component of the velocity:

$$u(r_0,t) = \frac{12\pi\eta}{(3+4\pi\eta)r^2(r_0,t)}\int_0^{r_0}\xi^2 R^2(\xi,t)\frac{\partial}{\partial t}R(\xi,t)d\xi \qquad (22)$$

The momentum equation in the Lagrangian formulation is found to be:

$$C_p(r_0,t) = \frac{-6}{3+4\pi\eta}\int_{r_0}^{A_0}\frac{g(\xi,t;C_p)+r(r_0,t)u^2(r_0,t)}{r^4(r_0,t)}\xi^2 d\xi + C_{p,\infty}(t)+2g(A_0,t)/r(A_0,t)-u^2(A_0,t) \qquad (23)$$

where

$$g(\xi,t;C_p) = \frac{12\pi\eta}{3+4\pi\eta}\int_0^{\xi}[\tfrac{1}{2}R(\zeta,t)(\frac{\partial}{\partial t}R(\zeta,t))^2 - \frac{4}{\mathrm{Re}}\frac{\partial}{\partial t}R(\zeta,t) + \tfrac{1}{2}\sigma R(R^{-3k}(\zeta,t)-1) - \tfrac{1}{2}R(\zeta,t)C_p(\zeta,t) + \frac{2}{\mathrm{We}}(R^{1-3k}(\zeta,t)-1)]\zeta^2 d\zeta \qquad (24)$$

The initial conditions translate into:

$$u(r_0,0)=0\,;C_p(r_0,0)=0$$

$$R(r_0,0)=1\,;\frac{DR}{Dt}(r_0,0)=0$$

There are four functions to be determined: $r(r_0; t)$, $u(r_0; t)$, $C_p(r_0; t)$ and $R(r_0; t)$. The equation for C_p is implicit and needs to be solved iteratively. Finally R is calculated, using an appropriate time integration from the Rayleigh-Plesset equation.

The numerical procedure used is similar to the one used by Wang and Brennen [1999]. It employs an explicit Euler time integration technique to obtain the bubble wall velocity from the bubble wall acceleration, and the Heun technique to obtain the bubble wall radius. The procedure is discussed below.

1. From initial and boundary conditions, or from previous time step, the following set of data is available:
   $R(r_0; t)$, $(\partial/\partial t)R(r_0; t)$ and $(\partial^2/\partial t^2)R(r_0; t)$
2. Using an explicit Euler time integration technique, we find
   $(\partial/\partial t)R(r_0; t+\Delta t) = (\partial/\partial t)R(r_0; t) + \Delta t(\partial^2/\partial t^2)R(r_0; t)$

For the bubble radius we find using Heun's method:

$R(r_0; t+\Delta t) = R(r_0; t) + \tfrac{1}{2}\Delta t[(\partial/\partial t)R(r_0; t) + (\partial/\partial t)R(r_0; t+\Delta t)]$

3. The fractional change of R is checked and if it is too large the time step Δt is adjusted and step 2 is repeated. When the fractional change of R is within limits, one is able to integrate equations (21) and (22) to find: $r(r_0; t+\Delta t)$ and $u(r_0; t+\Delta t)$
4. One is now able to iterate equation (23) to find $C_p(r_0; t+\Delta t)$. The final step is to use the Rayleigh-Plesset equation (13) to find: $(\partial^2/\partial t^2)\ R(r_0; t+\Delta t)$.

All quantities are now known at the new time step. One can repeat this sequence of steps for a new time step until time has progressed to the desired time.

The integrals in Eqs. (21)-(24) are evaluated using the midpoint (trapezoidal) rule.

In the time stepping procedure the bubble radius is computed as indicated above. Then the new bubble radius is compared to the one obtained in the previous time step. When the radius is within limits the computation may proceed. If the maximum fractional change is out of limits, the time step is halved and the bubble radius at the new time is re-calculated. Again it is checked. When the bubble collapsed and is in its rebound, the magnitude of the bubble wall acceleration decreases and a very small time step is now slowing down the computation unnecessarily. The time step needs to be increased again. When the fractional change of the bubble radius is within certain limits, say no more than 1%, the time step is doubled. After this adjustment, the bubble radius needs to be re-calculated and re-checked.

RESULTS

The values of the parameters that are kept fixed for all simulations the following ones of Wang & Brennen [1999]
R_0 = 100 μm; U_0 = 10 m/s; S = 0.0728 N/m; ρ_L = 1000 kg/m^3 and μ_E = 0.035 Pas. This gives for the Reynolds number: Re = 28.57, and for the Weber number: We = 137.4.
For the cavitation number, two values are used: σ = 0.4 and σ = 0.45. In this section a dimensionless cloud radius of A_0 = 100 is

used. The parameters that are varied are the pressure perturbation period t_G and the initial void fraction α_0. The pressure perturbation period will be varied between values ranging from 250 to 1000. For the initial void fraction α_0 the range is 0.01% up to 5%. In the Rayleigh-Plesset equation due to bubble-bubble interaction is of the order α_0. This is to be kept in mind for the higher initial void fractions.

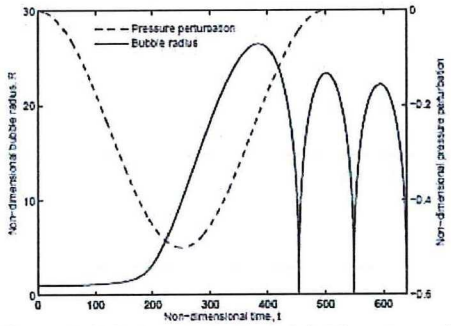

Figure 4: Solution of the Rayleigh-Plesset equation for a single bubble subjected to a decrease in ambient pressure followed by a subsequent ambient pressure recovery for t_G = 500, Cp_{min} = -0.5, σ = 0.4, Re = 28.57, We = 137.4.

Single bubble

Figure 4 shows the solution of the Rayleigh-Plesset equation for a single bubble subjected to a temporary drop in ambient pressure as shown in the same figure. A solution for a single bubble is obtained by excluding the continuum mixture equations and just solve for the Rayleigh-Plesset equation. The behavior of a single bubble in the far-field, as shown in Figure 4, serves as a reference for comparison with the behavior of individual bubbles in a cavitating/collapsing cloud.

Bubble cloud

Figure 5 shows the result for a bubble cloud subjected to a pressure perturbation of the type shown in figure 3 for a specific choice of the two parameters: t_G and C_{pmin}.

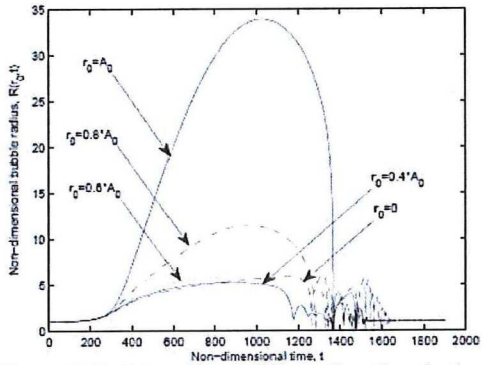

Figure 5: Bubble radius at different locations in the cloud subjected to a pressure perturbation shown in figure 3 for t_G= 1000, α_0= 0.1%, σ = 0.4, C_{pmin} = -0.7, Re = 28.57, We = 137.4, A_0 = 100.

In figure 5 the bubble radius is plotted for a situation t_G = 1000 and α_0 = 0:1%. Shown is the bubble radius at different radii of the cloud as function of time. It is seen that the bubbles at the cloud boundary attain the largest bubble radii. This happens when the pressure perturbation is completely recovered, thus after t_G = 1000. After this recovery, the collapse process starts. Note that the bubbles near the cloud boundary grow to a much larger size than the most inner bubbles. This is a phenomenon generally seen in cloud cavitation simulations. The large difference between growth rate of inner and outer bubbles is a function of the initial void fraction, and therefore can be related to bubble-bubble interaction effects. Simulations for higher and lower void fractions show that the stronger the bubble interaction, the smaller the difference in growth rate

Bubble interaction effects render the results of the simulations invalid if they are too strong. Therefore the 'cloud interaction parameter' is used, defined as:

$$\beta \equiv \alpha_0(1-\alpha_0)\frac{A_0^2}{R_0^2} \tag{25}$$

From this it can be seen that a high initial void fraction α_0 yields high bubble interactive effects (with a maximum at α_0 = 0:5), but also the cloud radius A_0 increases β.

α_0	A_0=30	A_0=100	A_0=300
0.01%	0.09	0.99	8.99
0.1%	0.89	9.99	89.91
1%	8.91	99.99	891.00
5%	42.75	475.00	4275.00

Table 1. Cloud interaction parameter for various α_0 and A_0

As is shown in table 1 the β value for figure 5 is intermediate at a value of approximately 10.

Figure 5 shows that the collapse process starts near the middle of the cloud radius, near $r_0 = 0.6A_0$. For later times the center the collapse heads in both directions, toward the center of the cloud and towards the cloud boundary.

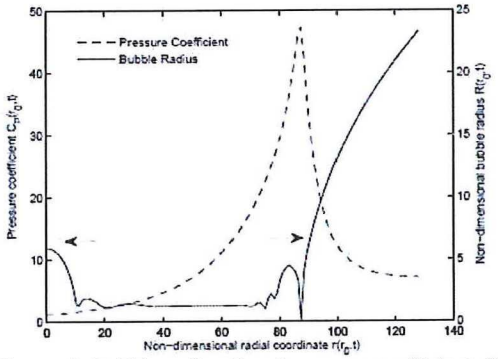

Figure 6: Bubble radius R and pressure coefficient C_p as function of radial coordinate r at time t = 1325.4 in Fig. 5.

Figure 6 shows the bubble radius distribution as function of location in the cloud, some time after the first bubble collapse, i.e. for dimensionless time t = 1325:4. It can be clearly seen that there is a collapse front traveling in the directions indicated by the arrows. In the collapse front traveling towards the cloud boundary, some secondary collapses and rebounds are observed

as well. Also included in figure 6 is the pressure coefficient. It is noticed that a pressure peak results from the small bubble radius near $r = 87$. This pressure peak is broad, in the sense that neighboring bubbles experience an elevated pressure as well. The Rayleigh-Plesset Eq. (13) shows the influence on the bubble wall acceleration of the neighboring bubbles. The right most neighbor that is going to collapse next experiences a higher negative acceleration due to the elevated pressure. The left most neighbor that is rebounding also experiences a negative acceleration due to the elevated pressure, and thus slowing the rebound and decreasing the maximum rebound radius.

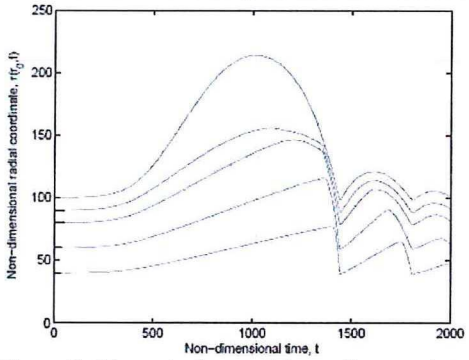

Figure 7: Dimensionless radial coordinate r plotted against dimensionless time t, for $t_G = 1000$, $\alpha_0 = 5\%$, $\sigma = 0.4$ and $C_{pmin} = -0.7$. Re = 28.57, We = 137.4, $A_0 = 100$

The location of the bubbles, is shown in figure 7, where r is plotted time for various values of r_0, for $\alpha_0 = 5\%$, $t_G = 1000$, $\sigma = 0.4$ and $C_{pmin} = -0.7$. Clearly at the cloud boundary, a large expansion of the cloud takes place. After the pressure perturbation recovery the cloud shrinks. The cloud collapses only to a size comparable to its initial size, i.e. prior to the pressure perturbation. It should be noted, however, that inside the cloud, local void fractions reach very low values, as was seen in Figs. 5 and 6.

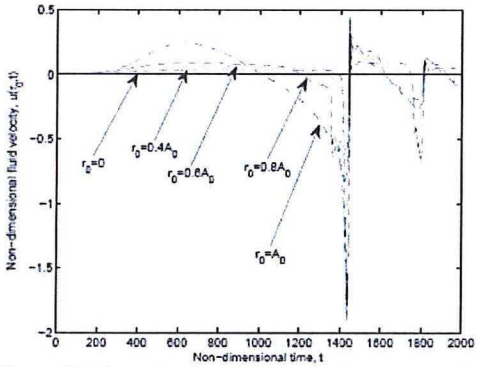

Figure 8: Dimensionless radial velocity u versus dimensionless time t for various values of r_0, for $t_G = 1000$, $\alpha_0 = 5\%$, $\sigma = 0.4$ and $C_{pmin} = -0.7$. Re = 28.57, We = 137.4, $A_0 = 100$

The mixture radial velocity inside the cloud, presented in Fig. 8 shows that the growth of the bubbles causes a small radial velocity in positive r-direction. A collapsing bubble, however, causes a considerable higher inward velocity. As the bubble collapses more violently, the change in velocity becomes faster and the negative velocities become even more negative. A discontinuity appears when the inward traveling front reaches the center of the cloud. Here the velocity changes sign.

One of the most interesting aspects of cloud cavitation for practical reasons is the noise and damage potential. Therefore, the radiated acoustic pressure in the far field has been calculated from the cloud's volumetric accelerations. The expression used follows from Eq. (5) with V the volume of the cloud. In dimensionless form we obtain ($\hat{p}_a = (r/D)\, p_a / \frac{1}{2}\rho_L U_0^2$):

$$p_a(t) = \frac{2R_0}{D}\left[2A(t)\left(\frac{dA(t)}{dt}\right)^2 + A(t)^2 \frac{d^2A(t)}{dt^2}\right] \qquad (26)$$

Here is a macro length scale corresponding to a typical length scale like the chord length of a hydrofoil. A typical result is shown in Fig. 9.

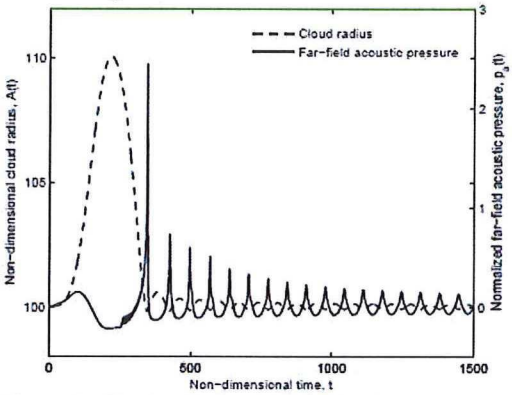

Figure 9: Cloud radius and far-field radiated acoustic pressure for $t_G = 200$, $\alpha_0 = 0.8\%$, $\sigma = 0.4$ and $C_{pmin} = -0.7$. Re = 28.57, We = 137.4, $A_0 = 100$

In this figure the far-field radiated acoustic noise $p_a(t)$ is plotted as well as the cloud radius $A(t)$. It is clear that the largest peak occurs when the cloud radius is minimum, thus at the first cloud collapse. The peaks of the secondary collapses are much lower and after some time the cloud starts oscillating in its eigenfrequency.

Verification

The model as implemented in the present study behaves fairly similar to the one presented in the literature. There is a good agreement of the bubble radius as function of time. The maximum bubble radius and the time of collapse are very similar. As clouds collapse a collapse front is formed, sometimes moving inward, sometimes moving outward and sometimes moving in both directions. The general effect is that when this front progresses the collapses get more severe, reaching their most violent point at one of the ends of the domain. In cases for which this collapse is most violent the rebound behavior found in the present study does not correspond to the one found in the literature. When the collapse process starts, the rebounds are very similar, but after some time the bubbles grow to a much larger size than found in corresponding cases in literature, see van Loo (2011).

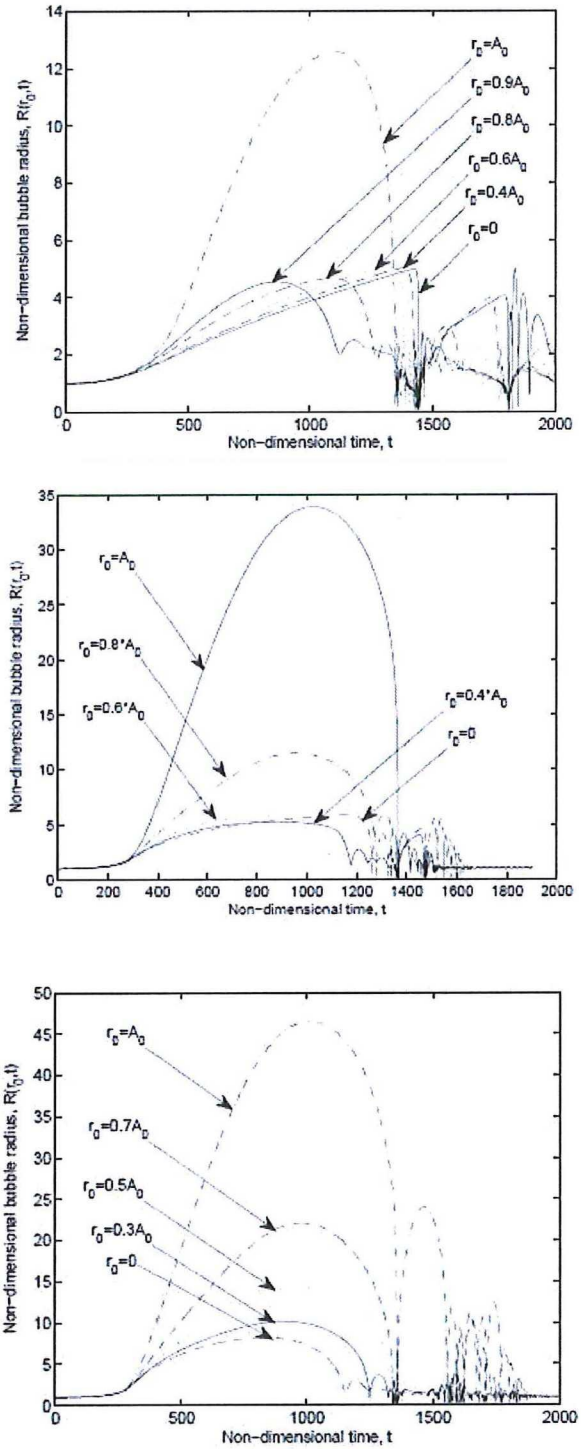

Figure 10: Bubble radius at different locations in the cloud subjected to pressure perturbation (Fig. 3) with t_G= 1000, C_{pmin} = -0.7. σ = 0.4, Re = 28.57, We = 137.4, A_0 = 100. Initial void fraction, α_0 = 5% (top), 0.1% (center) and 0.02% (bottom)

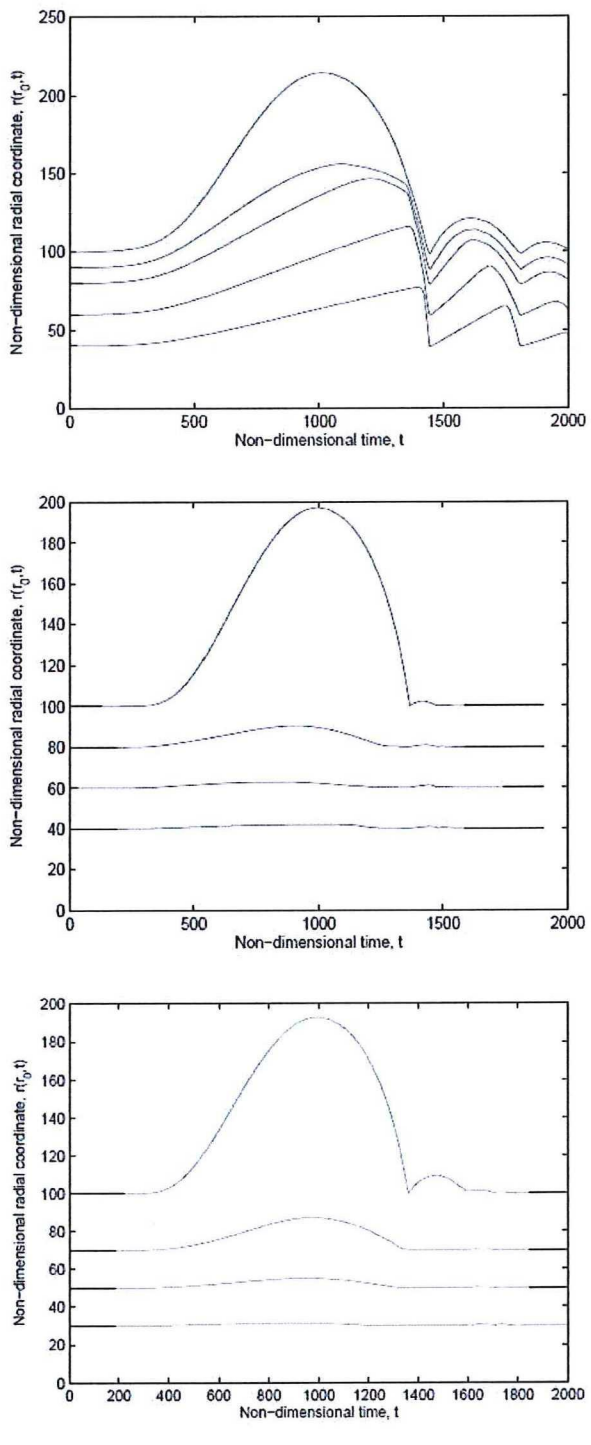

Figure 11: Radial coordinate r versus dimensionless time t, for t_G = 1000, C_{pmin} = -0.7, σ = 0.4, Re = 28.57, We = 137.4, A_0 = 100. Initial void fraction, α_0 = 0.02% (top), 0.1% (center) and 5% (bottom)

Discussion

Consider Fig. 10 which shows the bubble radius as function of time for the same cavitation number, and the same pressure perturbation period and amplitude but for three different initial void fractions, 0.02%, 0.1% and 5% (note that this corresponds to cloud interaction parameter β of. O(1), O(10) and O(100), respectively). As discussed above the bubbles near the cloud boundary have a higher growth rate than the inner bubbles. For each of the initial void fractions this 'shielding' effect is observed. However, for low initial void fractions the growth rate of the outer bubbles is much larger than for high void fractions. This is due to bubble-bubble effects. For high initial void fractions, bubbles are more closely packed, and thus interact stronger. Bubbles are slowed down in their growing process because their neighbor is in the way. This is not the case for the growth of the cloud radius. The cloud grows to roughly the same size for each of the initial void fractions considered, and appears to depend mainly on the pressure perturbation period t_G, not so much on initial void fraction α_0.

Fig. 11 shows the motion of the Lagrangian nodes at different initial locations r_0 in the cloud for initial void fractions α_0 of 5%, 0:1% and 0:02%. The difference in bubble interactive effects is very clear. For the lower initial void fractions the boundary bubbles grow to very large size while the inner part of the cloud is more or less stationary. For the high initial void fraction this is not the case. The mixture in the entire cloud moves outward as the cloud reacts to the pressure perturbation. After growth, the cloud collapses coherently. Also the rebounds are more coherent and larger than for the other two cases.

To inspect the behavior of the cloud boundary in more detail consider Fig. 12. In this figure the cloud boundaries for the three cases of Figs. 10 and 11 are shown. It is seen that the higher the initial void fraction, the earlier the cavitation starts and the later the collapse starts. Also the cloud reaches a larger maximum radius for higher initial void fractions. The cloud with the intermediate void fraction has the smallest rebound. This is because the inward and outward traveling collapse fronts cancel each other. Also, the secondary rebound period is considerably longer for higher initial void fractions. Bubbles effectively influence the frequency of the cloud as the cloud rebound frequency is considerably lower than that of an individual bubble.

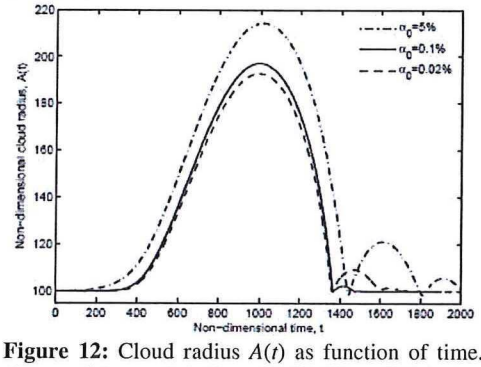

Figure 12: Cloud radius $A(t)$ as function of time. t_G = 1000, C_{pmin} = -0.7, σ = 0.4. Re = 28.57, We = 137.4, A_0 = 100 Initial void fraction, α_0 = 0.02%, 0.1% and 5%

For high initial void fractions the collapse process starts near the cloud boundary (due to the momentum of the growth of the outer bubbles, these can keep on growing and collapse slightly later) and then the collapse process moves inward. The shielding effects cause the outer bubbles to grow faster. However, it also keeps the inner bubbles from 'feeling' the ambient pressure recovery and therefore these bubbles keep growing even if the collapse process has already started. When the collapse front moves inward, it experiences a strong increase in local pressure peak. For a low initial void fraction the collapse process starts in the interior of the cloud. Again, the shielding effect makes that the outer bubbles have a much larger growth rate than the inner bubbles. The outer bubbles build up enough momentum to keep on growing even if the ambient pressure is recovered. Therefore the collapse starts in the center of the cloud. A collapse front is again noticed to be present, this time traveling outward. The focusing of pressure peaks is much smaller however, which can be seen in the rebound behavior. The rebounds are much smaller and are damped very quickly following cloud collapse.

The case of the intermediate initial void fraction shows a combination of the characteristics observed for the high and low initial void fractions. The collapse starts somewhere in the middle of the cloud and a collapse front travels both inward and outward (see Fig. 6). The inward moving front experiences some pressure focusing, however, this appears to cancel the outward moving front. The cloud collapse is the least severe of all cases.

COUPLING TO RESULTS OF RANS METHOD

At present RANS methods have not yet developed to the point that they can predict cavitation erosion. Predicting erosion demands accurate knowledge of radiated pressure waves from collapsing cavities or cavity clusters. These pressure waves are radiated in very short periods of time. RANS methods employ time-averaging. Thus the smallest time-scales are not represented. In this way, unless very small time steps are taken, RANS methods might not resolve the actual pressure peaks. Also predicting the details of a cloud collapse are computationally demanding. Bubble interaction effects and resulting shock waves are computationally costly. These effects that inherently influence the radiated acoustic pressures are not represented in RANS methods. The present model does take into account the small time scales. Time steps of 1 femtosecond are not uncommon. Also bubble interaction effects are taken into account and the resulting complex cloud collapse phenomena are represented. This gives the possibility to be able to recognize situations for which violent and potentially dangerous cloud collapses are to be expected. Also a quantitative estimate of radiated acoustic pressure results from the present model. Therefore a combination of both methods would give a more complete prediction of radiated pressures. It should be noted that the model of this study does not take into account the presence of a solid wall in the vicinity of the collapsing cavity cluster. However, from the literature (see Isselin et al. [1998]) it is known that a wall that is positioned closely to a collapsing cavity, decreases the radiated pressure waves. So it can be expected that the present model overestimates radiated pressure

waves. It should also be mentioned that yet another model is needed, namely for modeling the reaction of the material of the solid wall, however, this is beyond the scope of the present study.

In order to explore the possibilities of coupling the present model to a RANS method an example case is studied. The case is considered of a NACA0015 hydrofoil at 8 deg angle of attack. The chord length of the hydrofoil is c = 0.6m, the free stream velocity is U_0 = 17.71m/s and the cavitation number is σ = 1.43. Results of a RANS method (FRESCO) are found in Fig. 13.

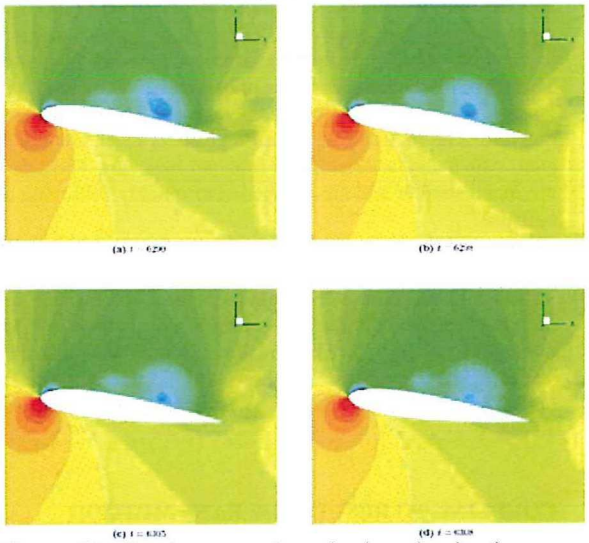

Figure 13: Development of a cloud cavity in time on a NACA0015 hydrofoil at an angle of attack of 8 deg. Re =10M, σ = 1.43.

In Fig. 13, the colors represent the pressure coefficient, red for high pressure and blue for low pressure. In the blue region, where the pressure is low, the black contour lines are lines of constant void fraction. The outer contour line in Fig. 13a represents a void fraction of 5% and the step to the next line is 5%. Thus in the middle of the cloud the maximum void fraction is 35%. In Fig. 13b, 0.2 milliseconds later, two inner contour lines have disappeared and the maximum void fraction is 25%. The cloud is collapsing and the local void fractions decrease. The lowest pressure in the cloud is C_{pmin} = -1.43. Figure 13d shows the situation just before the cloud disappears. The total time between first and last sub-figure is 0.45 milliseconds. This corresponds to a non-dimensional time of 79.70 (non-dimensionalized with velocity 17.71 m/s and initial bubble radius R_0 = 100μm). In the next time step, the cloud has vanishes; after a non-dimensional time of 92.97 (0.53 milliseconds). The pressure coefficient at that moment is C_p = -1:275.

Cavitation equilibrium cloud

The model requires the computation to start from an equilibrium situation. Therefore it the first task is to create a cavitated cloud with a mean void fraction comparable to the cloud in the RANS computations. It is chosen to create a cloud with a mean void fraction of 25%, since the cloud from RANS has the high void fraction of 35% only in a small part in the middle. From the equation for the void fraction (see Eq. (7)) it follows:

$$\alpha = \frac{\eta \frac{4}{3}\pi R^3}{1+\eta \frac{4}{3}\pi R^3} \tag{27}$$

so that

$$\eta = \frac{3}{4\pi R^3}\frac{\alpha}{1-\alpha}$$

Since the bubble distribution η is constant, the right-hand side is evaluated for the initial time, for which R = 1. This gives:

$$\eta = \frac{3}{4\pi}\frac{\alpha_0}{1-\alpha_0}$$

Substituting the equation for η in the one for α, yields:

$$\langle R\rangle^3 = \frac{\alpha(1-\alpha_0)}{\alpha_0(1-\alpha)} \tag{28}$$

Here $\langle R\rangle$ represents an expression for the mean bubble radius of the equilibrium cloud as a function of local void fraction and the initial void fraction. Now one can compute the mean bubble radius in the cloud in order to create a cloud with a void fraction of 25%. However, the initial void fraction is still not known. Note that the bubble radius is also a function of pressure. Therefore it is necessary to consider the equation for the pressure coefficient. Assuming that the system is in equilibrium one can write for the pressure coefficient equation (see Eq. (23)):

$$\frac{\partial}{\partial r}C_p(r_0,t) = \frac{-6}{3+4\pi\eta R^3(r_0,t)}\frac{\partial}{\partial t}u(r_0,t)\frac{\partial}{\partial r_0}r(r_0,t) = 0$$

This shows that the pressure is constant over the entire cloud. The pressure must thus be equal to the pressure at the boundary. The boundary condition reads, see Eq. (16):

$$C_p(A_0,t) = C_{p,\infty}(t) + \frac{2}{r(A_0,t)}\frac{d}{dt}[r^2(A_0.t)u(A_0.t)] - u^2(A_0.t)$$

For an equilibrium situation one finds:

$$C_p(r_0,t) = C_{p,\infty}(t)$$

A cloud in equilibrium has a constant pressure which is equal to the ambient pressure. From this one can conclude that $\langle R\rangle$ = R_{eq}, where R_{eq} is the value of the radii of the bubbles in a cavitated cloud in equilibrium. The Rayleigh-Plesset equation gives the relationship between pressure and bubble radius. For an equilibrium situation the time derivatives are absent and one finds from Eq. (13):

$$\frac{\sigma}{2}(R_{eq}^{-3k}-1) + \frac{2}{\mathrm{We}}(R_{eq}^{-3k} - R_{eq}^{-1}) - \frac{1}{2}C_{p,\infty} = 0 \tag{29}$$

The bubble radius is thus a function of cavitation number, Weber number and ambient pressure, but the initial void fraction does not appear in this expression. Assuming that the ambient pressure coefficient equals the negative of the cavitation number ($C_{p,\infty}$ = -σ), the relation between bubble radius and cavitation number is plotted in Fig. 14. Since the cavitation number and pressure coefficient are known, the equilibrium bubble radius can be computed. For the current case for which σ = 1.43, so $C_{p,\infty}$ = -1.43, the corresponding equilibrium bubble radius is R_{eq} = 3.39. Now there is only one unknown: the initial

void fraction. This can be computed from Eq. (28) and is for a cloud with a mean void fraction of 25%: α_0 = 0.84%. So if an ambient pressure decrease is imposed to a cloud of nuclei with α_0 = 0.84%, in which the ambient pressure will stay at $C_{p,\infty}$ = -1.43, for a flow with σ = 1:43 the bubble radii in the cloud will eventually all become equal to R_{eq} = 3.39. This cloud has a mean void fraction of 25%. This will be the equilibrium cloud used in the comparison with the cloud from the RANS solution. The relationship between equilibrium bubble radius, initial void fraction and mean cloud void fraction is given in table 2.

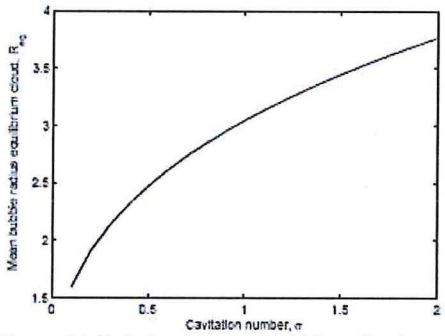

Figure 14: Relation between bubble radius in a cavitated cloud in equilibrium and cavitation number. Note that this relation is independent of initial void fraction. $C_{p,\infty} = -\sigma$

R_{eq}	α_0=1%	α_0=0.1%	α_0=0.01%
1	1	0.1	0.01
2	7.5	0.79	0.08
3	21.4	2.6	0.2
4	39.2	6	0.6
5	55.8	11.1	1.2
6	68.5	17.8	2.1
7	77.6	25.5	3.3

Table 2: Mean void fraction in cloud as function of mean bubble radius for three different initial void fractions. Values in percentages

To obtain the cloud prescribed above, the ambient pressure is decreased slowly using a ramp-up function up to the time it reaches the desired value of $C_{p,\infty}$ = -1.43. Subsequently this value is kept fixed until the cloud is stationary. The result of this simulation is shown in Fig. 15. It is observed that after sufficient time has passed, the bubbles oscillate coherently and the oscillations are no longer decreasing in amplitude, i.e. the cloud is oscillating in its natural frequency.
However, the amplitude of the oscillation is not zero, but assumed small enough that the cloud may be assumed to be in `semi-equilibrium'. This cloud is the initial condition for the collapse computation.

Equilibrium cloud collapse

The cloud constructed above is subjected to an ambient pressure recovery. This recovery should match the pressure coefficient development of the RANS method. For this example two cases are computed. In one case, the pressure recovery is specified as a cosine back to zero, in a non-dimensional time of 500. In the second case the ambient pressure is brought from -1.43 to -1.275 in a non-dimensional time of 92.97 and then stays at that value, see Fig. 16.

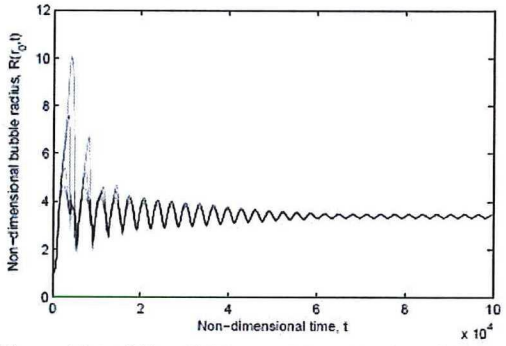

Figure 15: Bubbles (different r_0) in a cloud evolving to an equilibrium situation. σ = 1.43, α_0 = 0.84% and $C_{p,\infty}$ = -1.43.

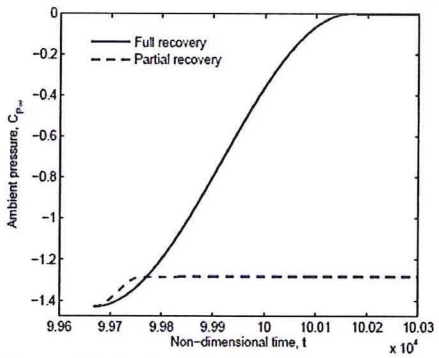

Figure 16: The 2 ambient pressure recovery cases

The results are shown in Fig. 17 for the bubble radii different locations in the cloud. The results are given for the same time domain, starting at the end time in the computation for the equilibrium cloud. The non-dimensional time that passes is 600 for both imposed pressure recovery functions. It should also be mentioned that the cloud starts with a radius of A = 110.22, which corresponds to a mean void fraction of α_0 = 25.94%, 1 percent higher than computed, due to the small oscillations of the semi-equilibrium cloud, see Fig. 15. Looking at the results, two apparent differences are noticed. The first is the time between first and second rebound (cloud frequency). The ambient pressure recovery from $C_{p,\infty}$ = -1.43 to 0, over a relatively long time, results in a cloud that collapses around the same time as for the short and partial pressure recovery from $C_{p,\infty}$ = -1. 43 to -1.275. Following this phase, the rebound frequency for the first case is much higher because of the higher ambient pressure. Also notice the maximum rebound radius of both bubbles and cloud itself. For the short and partial pressure recovery, bubbles rebound to higher values because the ambient pressure is still low.

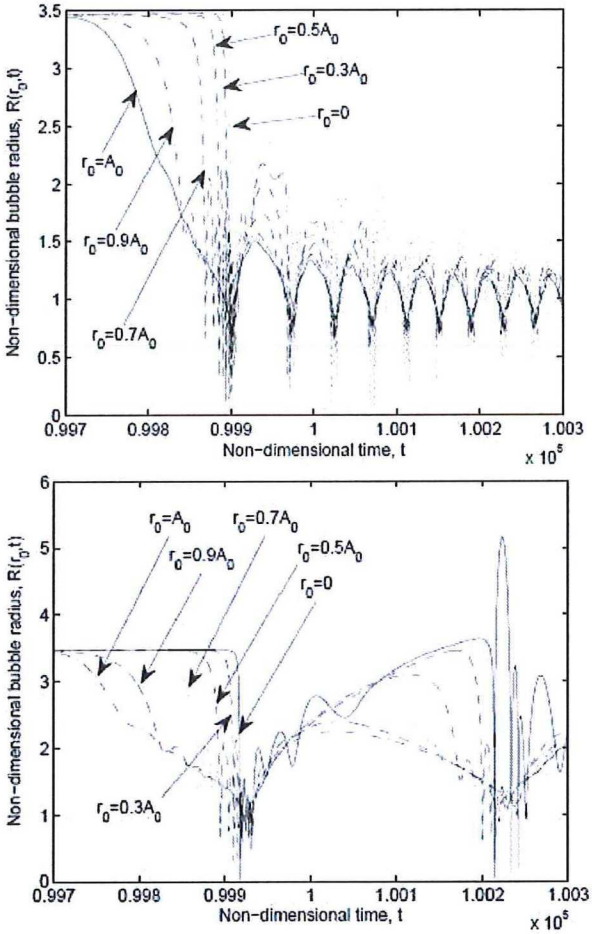

Figure 17: Bubble radii in a cloud of cavitated bubbles in equilibrium subjected to an ambient pressure recovery.
Top: slow recovery from $C_{p,\infty}$ = -1.43 to 0 (solid line in Fig. 16).
Bottom: fast but partial recovery from $C_{p,\infty}$ = -1.43 to -1.275 (dashed line in Fig. 16). $\alpha_0 = 0.84\%$, $A_0 = 100$, $\sigma = 1.43$.

The cloud radius and radiated acoustic pressure are presented in Fig. 18. Indeed, the cloud rebounds to a larger size for the case for which the ambient pressure recovery is only partial. Furthermore, the radiated acoustic pressures are considerably higher for the case for which the ambient pressure recovers to zero. Also in this case, higher peaks are attenuated longer, even with the higher rebound frequency. The definition of the cloud interaction parameter β (Eq. (25)) indicates that the cloud radius has a large influence on its behavior. The present results are for a cloud radius of $A_0 = 100$. From Fig. 13 it is estimated that, in comparison with the chord of 0.06m, the cloud is 0.01m in diameter. This corresponds to a non-dimensional cloud radius of $A_0 \approx 55$. This yields $\beta \approx 25$ compared to $\beta = 83.3$ used in the computation. One should thus expect smaller bubble interactive effects than the results show.

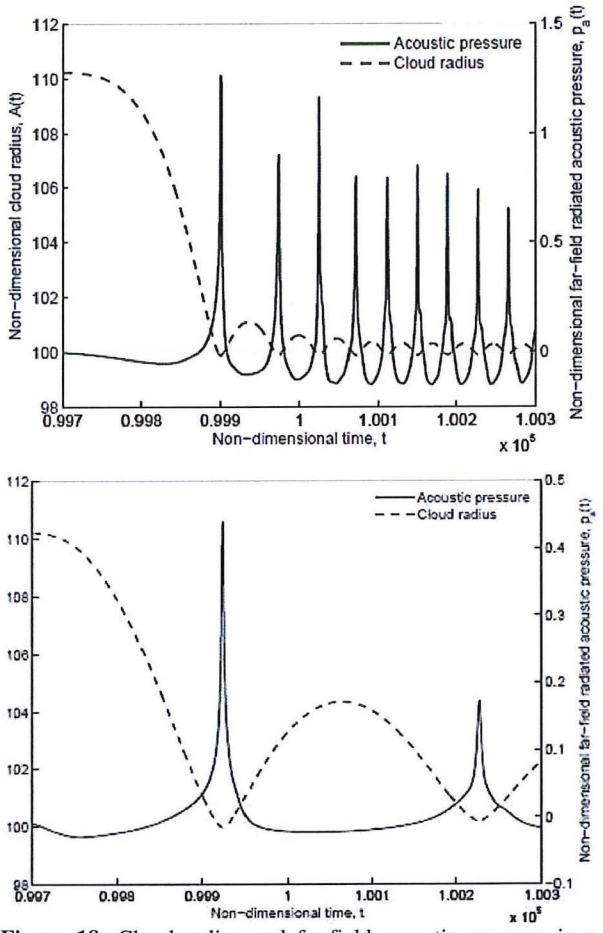

Figure 18: Cloud radius and far-field acoustic pressure in a cloud of cavitated bubbles in equilibrium subjected to an ambient pressure recovery.
Top: slow recovery from $C_{p,\infty}$ = -1.43 to 0 (solid line in Fig. 16).
Bottom: fast but partial recovery from $C_{p,\infty}$ = -1.43 to -1.275 (dashed line in Fig. 16). $\alpha_0 = 0.84\%$, $A_0 = 100$, $\sigma = 1.43$.

Discussion

It appears possible to couple bubble cloud method with the RANS method, however, some considerations have to be taken into account.

- A procedure has been developed to construct a cloud to match a shed cloud computed using a RANS method. Since the bubble cloud method is formulated in Lagrangian coordinates, it considers a cloud that is convected with the free stream velocity.
- The cloud interaction parameter β corresponding to the result of the RANS method is not equal to the one of the bubble cloud method, due to the difference in cloud radius. The present bubble cloud method yields too strong bubble interaction effects. This parameter should have matched better.
- The initial void fraction determined for the bubble cloud method should match the void fraction of the RANS method upstream of the cloud. The initial void fraction is the only

parameter that can be varied to achieve a cloud with the desired mean void fraction. Therefore, the initial void fraction of the RANS results should match that of the present model, not the other way around.
- For quantitative values of the radiated acoustic noise the presence of a wall in the vicinity of a collapsing bubble cluster should be accounted for. The presence of the wall is expected to have reduced the radiated pressures. Experiments should confirm the found values

CONCLUSION

Results of the bubble cloud method have been obtained for ranges of various model parameters. It is concluded that the results are very dependent on the cloud interaction parameter β. This parameter contains three other parameters: initial void fraction α_0, initial cloud radius A_0 and initial bubble radius R_0. The latter dimensionless initial bubble radius is defined to be equal to unity. Initial void fraction α_0 and initial cloud radius A_0 have been varied. The resulting β varies over three orders of magnitude, which results in physically different behavior. For β of O(1) an radially outward traveling collapse front is formed. For β of O(10) two collapse fronts are formed, starting somewhere inside the cloud, traveling both inward and outward. These fronts tend to cancel each others pressure peaks and are the least violent. For still larger β, O(100), an inward traveling collapse front is formed that is observed to have a strong focusing effect towards the center of the cloud. This type of collapse is the most violent. A large cloud interaction parameter β is achieved for a relatively high initial void fraction: α_0 = O(1%) or higher, or for large cloud initial radius.

The pressure perturbation period is another important parameter. The longer a cloud is subjected to a low pressure, the more time the cloud has to cavitate, and the larger it can grow. Larger bubbles collapse more violently, and therefore the pressure perturbation period has a direct relation to the severity of the collapse. The precise function of time of the pressure perturbation does not appear to have a significant influence.
A cloud subjected to a sudden decrease in ambient pressure followed by a slow recovery, cavitates in a bigger volume than a cloud subjected to a slow decrease in ambient pressure and a sudden recovery.

Variations in Weber number or Reynolds number are found to have a small influence on the results. Decreasing the Reynolds number by slowing down the flow or adding damping in the effective viscosity μ_E results in the bubbles and the cloud growing to smaller sizes and tend to damp quickly after collapse.

It has proven to be possible to make a quantitative comparison between results of the bubble cloud method and results of a RANS method. A procedure has been developed to construct a cloud that is comparable to the vapor cloud shed from a sheet cavity and traveling downstream over a hydrofoil as obtained in a RANS computation. This equivalent cloud is then subjected to an ambient pressure recovery, which leads to a cloud collapse.
Since the initial void fraction and initial cloud radius have a large effect on the collapsing process, in the bubble cloud method these two parameters should match the corresponding ones of the RANS method

REFERENCES

C.E. Brennen. Cavitation and Bubble Dynamics. Oxford University Press, 1995.

R.B. Chapman and M.S. Plesset. Thermal effects in the free oscillation of gas bubbles. ASME J. Basic Eng., 93:373-376, 1971.

A.P. Dowling and J.E. Ffowcs Williams. Sound and sources of sound. Ellis Horwood Limited and John Wiley & Sons, 1983.

I. Hansson and K.A. Mörch. The dynamics of cavity clusters in ultrasonic (vibratory) cavitation erosion. Journal of Applied Physics, 51(9):4651{4658, 1980.

J. Isselin, A. Alloncle, and M. Autric. On laser induced single bubble near a solid boundary: Contribution to the understanding of erosion phenomena. Journal of Applied Physics, 84(10):5766-5771, 1998.

K.A. Mörch. Energy considerations on the collapse of cavity clusters. Applied Scientific Research, 38(1):313-321, 1982. ISSN 00036994.

J. Rubinstein. Bubble interaction effects on waves in bubbly liquids. Journal of Acoustical Society of America, 77 (6):2061{2066, 1985.

J.H. Seo, S.K. Lele, and G. Tryggvason. Investigation and modeling of bubble-bubble interaction effect in homogeneous bubbly flows. Physics of Fluids, 22:1-18, 2010.

S. van Loo. Numerical Study on the Collapsing Behavior of a Cavitating Cloud of Bubbles. MSc thesis, University of Twente, March 2011.

Y.C. Wang. Shock Waves in Bubbly Cavitating Flows. PhD thesis, California Institute of Technology, 1996.

Y.C. Wang and C.E. Brennen. Shock wave development in the collapse of a cloud of bubbles. volume 194, pages 15-19, 1994. ISBN 0791813776.

Y.C. Wang and C.E. Brennen. Numerical computation of shock waves in a spherical cloud of cavitation bubbles. Journal of Fluids Engineering, Transactions of the ASME, 121(4): 872-880, 1999. ISSN 00982202.